Cui *et al. Journal of Nanobiotechnology* (2025) 23:259
https://doi.org/10.1186/s12951-025-03269-2

Journal of Nanobiotechnology

RESEARCH Open Access

Plant volatiles-loaded core-shell micro-nano fibers to achieve efficient and sustained bisexual attraction to pests

Chenglong Cui[1†], Wenjie Shangguan[1†], Kebin Li[1], Xingfu Jiang[1], Zhimin Wang[1], Jiao Yin[1*] and Lidong Cao[1*]

Abstract

Background Chemical pesticides face significant challenges regarding their efficacy and environmental impact. Plant-based food attractants have emerged as a promising green alternative for pest control. However, their field application is limited by the short duration of effectiveness, necessitating improved carrier systems for sustained release. Electrospinning is a promising technology in this field, with core-shell fibers offering superior performance in efficient loading and sustained release compared to uniaxial fibers, highlighting their potential for further development.

Results In this study, core-shell micro-nano fiber mats were prepared via coaxial electrospinning using multiple environmentally friendly polymers. These mats were firstly and successfully loaded with food attractants bisexually attractive to *Loxostege sticticalis* adults, including 1-octen-3-ol, trans-2-hexenal, linalool, and anethole, enabling sustained release and effective trapping. The components in the core-shell spinning solution were chemically compatible, and after spinning, the poly(3-hydroxybutyrate-co-4-hydroxybutyrate)/polycaprolactone (PHB/PCL) in the shell layer and polyethylene oxide (PEO) in the core layer formed core-shell fibers with clear boundaries. The mats achieved an average encapsulation efficiency of 78% for active ingredients, with a sustained release profile that delivered over 60% of the attractants within 80 days while mitigating early burst release. Electroantennogram and behavioral studies revealed that the mats retained electrophysiological activity for at least 90 days, effectively attracting male and female adult insects even after 75 days. Field trials demonstrated that the mats significantly outperformed commercial slow-release carriers, attracting a higher number of *L. sticticalis* adults. Additionally, the mats exhibited strong stress resistance, biodegradability, and environmental compatibility, effectively protecting active molecules while minimizing ecological impact.

†Chenglong Cui and Wenjie Shangguan contributed equally to this work.

*Correspondence:
Jiao Yin
jyin@ippcaas.cn
Lidong Cao
caolidong@caas.cn

Full list of author information is available at the end of the article

Conclusions The developed fiber mats provide a highly efficient, eco-friendly carrier for plant-based food attractants, offering prolonged efficacy and improved insect trapping performance. This study highlights their potential for sustainable agriculture and pest management, paving the way for greener alternatives to chemical pesticides.

Graphical abstract

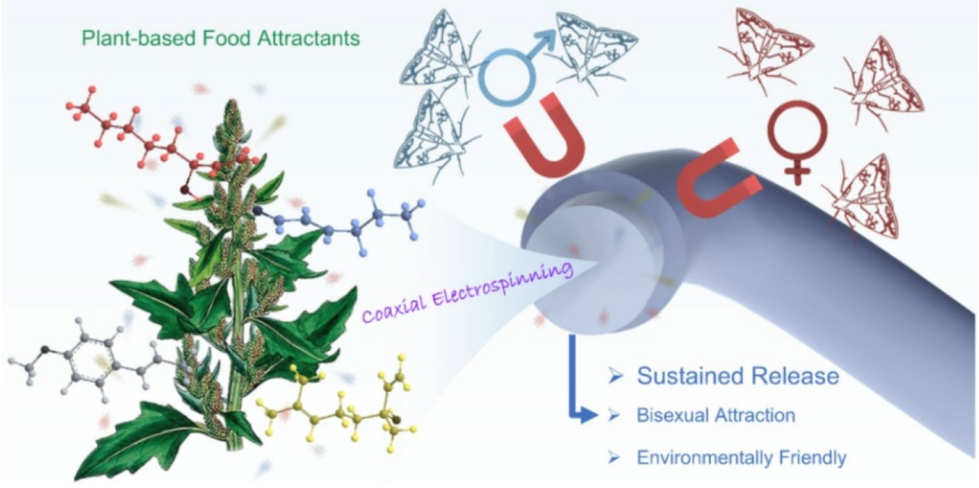

Keywords Food attractants, Micro-nano fiber, Sustained release, Coaxial electrospinning, Green pesticide

Background

Pollution and resistance linked to traditional chemical pesticides pose significant challenges to global agriculture [1, 2], with climate change exacerbating pesticide failure and reducing their efficacy [3]. Studies show that pesticides are becoming increasingly toxic to plants, invertebrates, and other non-target beneficial organisms, with even sublethal doses threatening insect species' survival [4–6]. Additionally, pesticide contamination of groundwater and soil is spreading globally [7]. These issues underscore the need for sustainable pest control solutions, particularly in the case of *Loxostege sticticalis* [8]. This Lepidoptera pest, classified as a first-class crop pest in China by the Ministry of Agriculture and Rural Affairs in 2020, ranks third on the national pest list and is expected to affect about 1.33 million hectares by 2024. The pest is widespread across regions between 36°N and 53°N, including parts of China, Mongolia, Russia, Kazakhstan, Ukraine, North America, and Europe. Its widespread impact highlights the urgent need for effective pest management strategies to protect global agriculture and mitigate environmental harm.

In long-term integrated pest management, eco-friendly and safe insect food attractants, such as yeast, protein, ammonia solution, bacteria, and plant volatiles, effectively trap pests and help control their populations [9, 10]. These attractants can be combined with traps or pesticides in an attract-and-kill strategy [11, 12]. As a green alternative to chemical pesticides, food attractants are widely used in various pest control scenarios, including farmland, woodlands, orchards, and grain storage, showing promising potential [13–16]. Volatile organic compounds (VOCs) from plant hosts, such as alcohols, aldehydes, esters, and terpenoids, are particularly attractive to herbivorous insects [17, 18]. Unlike insect sex pheromones, which attract mainly females, plant-based food attractants are more effective in targeting entire pest populations [19, 20]. However, the volatility of these compounds and the challenges posed by harsh field conditions make controlling their release kinetics difficult, limiting large-scale implementation of this strategy [21].

To improve the application potential of VOCs (such as insect pheromones, essential oils, and plant volatiles) in plant protection, research has focused on formulations and carriers that enhance their release performance [22–24]. Studies have explored passive dispensers [25], microcapsules [26], gels [27], and other carriers for plant volatile-based food attractants. Passive dispensers, like plastics and rubbers, load VOCs based on material permeability, but their limited biodegradability is a major drawback. Microcapsules and gels, which use polymer materials to encapsulate active ingredients, are influenced by factors like wall thickness, polymer cross-linking, porosity, and particle size, but their release duration often falls short of pest occurrence periods. Recent research suggests that micro-nano carriers significantly improve VOCs encapsulation, dispersion, and controlled release, enhancing biological activity [28]. Regrettably,

these promising laboratory research findings do not appear to have significantly influenced the formulations of these chemicals available in the market [29]. We believe this may be due to: (i) insufficient optimization of VOCs release behavior, such as sudden release; (ii) laboratory testing overlooked the effects of environmental factors. Therefore, designing carriers with improved release performance and conducting field research is crucial.

Electrospinning is a key method for producing micro-nano fibers, which offer excellent encapsulation, release performance, and functionalization potential [30, 31]. These fibers are widely used in biomedical applications, such as tissue engineering scaffolds, drug delivery, and wound dressings [32]. Recently, fiber carriers have gradually been developed for the loading, release and field application of insect sex pheromones [29]. Through polymer selection [33, 34], fiber structure optimization [35], and development of functional carriers [36], micro-nano fibers have greatly improved the practical use of VOCs. While micro-nano fiber carriers have not yet been applied to food attractants (Table S1), they show significant potential. Our previous research also demonstrated that core-shell fiber carriers, produced by coaxial electrospinning, offer strong encapsulation and effectively prevent the sudden release of pheromones [37]. Additionally, environmentally friendly polymers like polycaprolactone and polyhydroxybutyrate are used to create fiber carriers with good spinnability, biodegradability, mechanical properties, and controlled release capabilities, helping reduce agricultural microplastic pollution and biological toxicity risks [38].

In the early stage, we extracted and identified four active substances from the host plants that the *L. sticticalis* likes to feed on, such as *Chenopodium album* L., *Setaria viridis*, *Medicago sativa* L.: 1-octen-3-ol, trans-2-hexenal, linalool, and anethole. These VOCs were formulated as bisexually attractive food attractants to *L. sticticalis*. Herein, we employed coaxial electrospinning technology to select Poly(3-hydroxybutyrate-co-4-hydroxybutyrate) (PHB) and polycaprolactone (PCL) as shell, with polyethylene oxide (PEO) as the core, to load a food attractant composed of the aforementioned four components (Scheme 1). The fiber shell composed of PHB and PCL provided the fiber carrier with excellent stress resistance and protection, while the PEO offered good chemical compatibility with four VOCs, enabling effective encapsulation and loading. Notably, these polymers all exhibited good degradation properties. Moreover, the design of microscopic core-shell structures is expected to improve the undesirable release behavior of food attractants. The attractant-loaded core-shell fibers were systematically characterized, and their encapsulation/loading properties, release behavior,

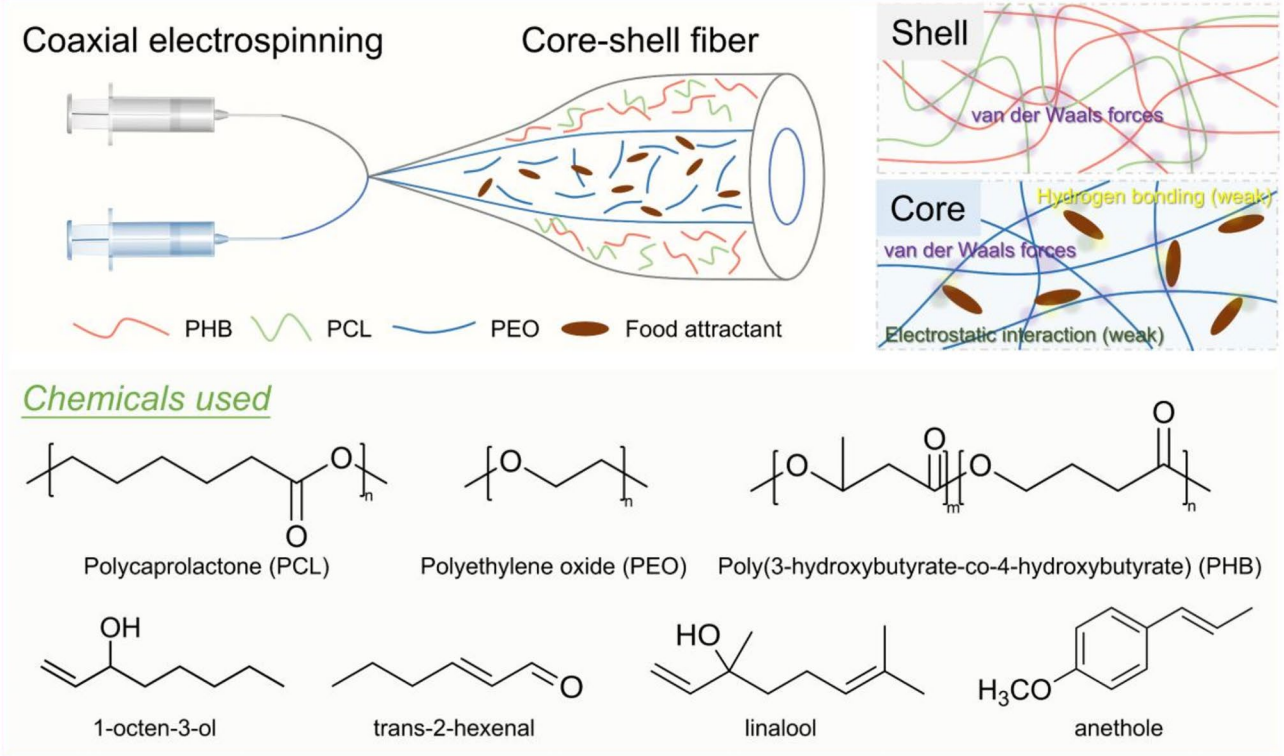

Scheme 1 Schematic illustration of the coaxial electrospinning process for preparing attractant-loaded core-shell fibers, along with the chemicals used and their potential chemical interactions within the micro-nano fibers

stress resistance, degradability and were investigated. The long-term bisexual attraction of this carrier system was verified through electroantennogram recordings and behavioral tests, and field trapping tests were conducted on *L. sticticalis*. This research will provide an insight for developing efficient and environmentally friendly food attractant carriers.

Methods

Materials

Chemicals 1-octen-3-ol (Mw = 128.21, purity 98.0%) was obtained from Yuanye Technology Co., Ltd. (Shanghai, China); trans-2-hexenal (Mw = 98.14, purity 98.0%) from Aladdin Biochemical Technology Co., Ltd. (Shanghai, China); linalool (Mw = 154.25, purity 96.0%) from Tokyo Chemical Industry Development Co., Ltd. (Shanghai, China); and anethole (Mw = 148.2, purity 98.0%) from MacLean Biochemical Technology Co., Ltd. (Shanghai, China). PHB (EM 5500 F; Mw = 750,000) was obtained from Shenzhen Ecomann Biotechnology Co., Ltd. (Shenzhen, China). PCL (Mw = 80,000) was obtained from Wokai Biotechnology Co., Ltd. (Beijing, China). PEO (Mw = 1,000,000) was obtained from Wokai Biotechnology Co., Ltd. (Beijing, China). Analytically pure chloroform was obtained from Beijing Reagent Factory. Dichloromethane (DCM) was purchased from Beijing Ouhe Technology Co., Ltd. (Beijing, China). The traps and commercially available polyethylene slow-release bottles (RS) used in the field experiments were obtained from Pherobio Technology Co., Ltd. (Beijing, China).

Insects The *L. sticticalis* population used in this experiment was a multi-generational population that was laboratory-reared. Larvae were placed in a glass flask and provided with fresh *C. album* L. regularly. The adult *L. sticticalis* were kept in a cage containing 10% honey water as a source of nutrition. The rearing conditions included a temperature of 25 ± 2 °C, a relative humidity of 75 ± 10%, and a photoperiod of L16:D8h.

Preparation of food attractant-loaded fiber mat

The core-shell fiber mats (FF), capable of loading food attractants, were prepared through electrospinning using an ET-2535X system (UCALERY Development Co., Ltd., Beijing, China). The electrospinning apparatus consisted of a power supply, a syringe pump, and a collector. Based on exploration of the spinning solution formulations (Figure S1), it was determined that 8% (*w*/v) PHB and 2% (*w*/v) PCL dissolved in chloroform served as the shell spinning solution. The core spinning solution consisted of 0.5% (*w*/v) PEO dissolved in DCM, with the addition of 100 mg of food attractant per mL of core solution. The food attractant comprised 1-octen-3-ol, trans-2-hexenal, linalool, and anethole in a ratio of 10:5:1:1. Both solutions were stirred at room temperature at a speed of 800 rpm for at least 8 h. Additionally, fluorescein isothiocyanate dye and rhodamine B were added to the shell and core solution at a concentration of 0.01 mg/mL, respectively, for the preparation of fluorescently labeled FF. The PHB/PCL mat was prepared by uniaxial electrospinning of the shell solution for subsequent comparative experiments.

The experimental parameters for coaxial electrospinning were as follows: the outer and inner diameters of the coaxial needles were Φ_{ext}/Φ_{int} = 1.8/1.3 mm for the external needle, and Φ_{ext}/Φ_{int} = 0.9/0.6 mm for the internal needle. The flow rates of the shell and core solutions were 0.38 mL/h and 0.08 mL/h, respectively. The applied positive voltage was 13.5 kV, with a negative voltage of 4 kV, and the distance between the needle and the collector was set to 25 cm. The temperature was maintained at 25 ± 3 °C, and the humidity was controlled at 45 ± 2%. The prepared mats were dried at room temperature (25 ± 2 °C) for 24 h before characterization.

Characterization of food attractant-loaded fiber mat

Fourier transform infrared spectroscopy (FTIR, NICOLET 6700, Thermo Scientific, Waltham, MA, USA) was conducted with a resolution of 4 cm^{-1}, within a wavenumber range of 600–4000 cm^{-1}, and 64 scans. X-ray diffraction (XRD, Bruker D8 Advance, Bruker, Karlsruhe, Germany) was performed using Cu Kα radiation, with a 2θ range of 10–60°. X-ray photoelectron spectroscopy (XPS, Thermo Scientific K-Alpha, USA) employed an Al Kα X-ray source (λ = 8.33 Å), using the C 1s peak at 284.8 eV as the reference signal for semi-quantitative analysis of the surface's external layers. An ultraviolet spectrophotometer (Shimadzu, UV-1800, Tokyo, Japan) was used to measure the absorbance of the fiber mat. Research-grade microscope (Olympus IX83, Olympus, Tokyo, Japan) was used to observe the morphology of the fiber mat under different light source voltages. Scanning electron microscopy (SEM, SU8010, Hitachi Ltd., Tokyo, Japan) was conducted at a working voltage of 10 kV, with a gold coating thickness of 8 nm. Fiber diameters were measured using ImageJ software, with the average diameter calculated across samples ($n \geq 100$). Transmission electron microscopy (TEM, JEM-2100Plus, JEOL, Japan) was carried out at an electron beam accelerating voltage of 80 kV. The fiber samples for TEM observation were collected in the spinning path using a copper mesh with a carbon film, and the collection time was about 3–5 s. Laser confocal microscopy (LSM 980, Zeiss, Germany) was used to examine the fluorescently labeled FF. Thermogravimetric analysis (TGA, PerkinElmer STA 8000, PerkinElmer, Waltham, USA) was performed to evaluate the thermal stability and decomposition behavior of FF and its components. The analysis was conducted by heating from 40 °C to 800 °C at a rate of 10 °C/min under a

nitrogen flow of 20 mL/min. The derivative thermogravimetry (DTG) curve was obtained by differentiating the TGA curve. The thickness of the tested fiber mats was 0.05 mm, and all tests were repeated a minimum of three times.

Loading and release performance

The loading and release performance of fiber mats are key factors determining their potential for application as food attractant carriers. First, 50 mg of the FF was weighed into a 5 mL volumetric flask, followed by the addition of methanol. The mixture was then ultrasonicated for 30 min, after which the encapsulation and loading efficiencies were analyzed using high-performance liquid chromatography (HPLC). To further evaluate the stability of the attractant in FF, the retention rates of samples stored at 4 °C, 25 °C, and 45 °C for 10 days were tested in a light-proof and sealed environment.

To evaluate the release performance of the FF, it was cut into 30 mg pieces and placed in a polyethylene centrifuge tube with an approximate diameter of 1.5 cm. The release experiment was conducted in a fume hood at room temperature under constant medium-speed ventilation conditions, with FF released naturally. Sampling was conducted at various time points, and the residual attractant content was quantified using HPLC and the external standard method. The method for extracting food attractants from fiber mats involved placing 30 mg of FF in a volumetric flask with methanol. After ultrasonic treatment for 30 min, the volume was adjusted to 5 mL, and 1 mL of the solution was filtered into an injection bottle for analysis. To analyze the release mechanism of food attractants in FF, various release kinetic models were employed to fit and evaluate the cumulative release rates at different time points. These models included the zero-order model, first-order model, Higuchi model, Ritger-Peppas model, and Weibull model, all of which aimed to reveal the release mechanism.

The HPLC test conditions were as follows: HPLC (1200-DAD, Agilent, Santa Clara, CA, USA) analysis utilized a ZORBAX SB-C18 column (4.6 × 250 mm, 5 μm). The mobile phase for 1-octen-3-ol was methanol: water (v/v) = 60:40, with a flow rate of 1.0 mL/min, an injection volume of 10 μL, a column temperature of 30 °C, and a diode array detector signal at 226 nm. The mobile phase for trans-2-hexenal was methanol: water (v/v) = 60:40, with a flow rate of 1.0 mL/min, an injection volume of 10 μL, a column temperature of 30 °C, and a diode array detector signal at 260 nm. The mobile phase for linalool was acetonitrile: water (v/v) = 55:45, with a flow rate of 1.0 mL/min, an injection volume of 10 μL, a column temperature of 25 °C, and a diode array detector signal at 210 nm. The mobile phase for anethole was acetonitrile: water (v/v) = 20:80, with a flow rate of 1.0 mL/min, an injection volume of 10 μL, a column temperature of 25 °C, and a diode array detector signal at 254 nm.

Stress resistance and degradability

The water contact angle meter (OCA 20, Data Physics, Germany) was used to measure the water contact angle (WCA) of the fiber mat. A 2 μL water droplet was placed on the FF surface, and the change in WCA was recorded over a period of 30 min until the droplet spread completely. The effect of humidity on FF was assessed by controlling humidity levels (100% and 50%) in an artificial climate chamber. Swelling rate: FF was immersed in water, and the sample was removed after 1 h, 6 h, 12 h, and 24 h. Excess surface water was gently absorbed with filter paper, and the weight was immediately measured. Solubility rate: FF was placed in a beaker and stirred at 500 rpm and 25 °C for solubility. The residual fiber mat was removed after 12 h, 24 h, 36 h, and 48 h, and weighed after ensuring it was completely dry. The swelling/solubility rate was calculated as follows:

$$Swelling/solubility\ rate\ (\%) = \frac{Weight\ after\ test - Initial\ weight}{Initial\ weight} \quad (1)$$

The reflectance of the FF was measured using a UV-vis-Infrared spectrophotometer (Hitachi, UH4150, Tokyo, Japan). The mats were cut to dimensions of 10 × 30 × 0.05 mm and reflectance was recorded over a wavelength range of 200–800 nm. All tests were repeated 3–5 times, and mean values were calculated for statistical analysis. UV weathering test: 50 mg of FF and filter paper (as a control) were weighed and placed in a UV aging box for 1 day, after which their retention rates were calculated of attractant. The light source was a xenon arc lamp with a wavelength of 340 nm and an irradiance of 0.76 W/m^2/nm. The exposure cycle consisted of 8 h of drying followed by 4 h of condensation.

To evaluate the mechanical properties of FF, they were measured by standard tensile test method. FF was cut into 25 mm × 13 mm pieces and subjected to tensile testing on a universal testing machine (Instron, Canton, MA). The grip spacing was set to 50 mm. During the test, the tensile stress-strain curves of the samples were recorded and compared with the PHB/PCL mats to analyze the differences in mechanical properties caused by the material composition.

Composting experiments were conducted on FF and RS for comparison. The samples were placed in soil with controlled humidity of 15%, temperature of 25℃ and the soil was silty loam (44.39% sand, 51.05% silt, and 4.56% clay) with an organic matter content of 16.75%. The samples were taken out and weighed at 1, 3, 5, and 7 days, and the degradation rate was calculated according to

the formula reported previously [39]. The changes in the morphology and chemical properties of FF at different time points were examined using SEM and FTIR, respectively. To evaluate the degradation performance of the FF, mats were regularly collected and observed throughout the field trial. In addition, FF was placed in a field environment to simulate actual application scenarios, and changes in its diameter were examined using SEM to further analyze its degradation behavior comprehensively.

Biological activity assay

Electroantennogram (EAG) recording Insect antennae are crucial structures for receiving and processing external chemical signals. To investigate the electrophysiological response of *L. sticticalis* antennae to FF, we used an EAG IDAC 4 system (Syntech, Buchenbach, Germany) to test the antennal potential responses of both male and female adults to freshly prepared FF. Specifically, the antennae were rapidly excised using a scalpel, and the antennal base was connected to the negative electrode using SPECTRA 360 electrode gel (Parker Lab, USA), while the tip was connected to the positive electrode. For each EAG recording, 200 mg of freshly prepared FF was folded into a rectangular shape (2 cm in length and 0.5 cm in width) and placed in a Pasteur pipette as the stimulus source after the solvent had evaporated. FF without attractant were used as the control. The stimulus, placed in the Pasteur pipette, was injected into a charcoal-filtered and humidified airflow for 0.2 s at a flow rate of 500 mL/min, delivered to the antennae by an air stimulus controller CS-55 (Syntech, Germany).

The antennal responses to the volatiles from the FF were recorded using a PRG-3 probe. The signals were processed with an IDAC-4 data acquisition controller and analyzed using EAG Pro software (Syntech, Germany). Additionally, we periodically tested the changes in electrophysiological responses of both male and female *L. sticticalis* to FF with varying release times under a fume hood. Each experiment was conducted with three biological replicates and three technical replicates.

Behavioral tests The olfactory behavioral responses of both male and female adults of the *L. sticticalis* were evaluated using an insect olfactory behavior selection apparatus (ZL2023204533809) to assess their indoor behavioral responses toward the FF. The olfactory behavior detection apparatus consists of a gas purification and humidification system, an atmospheric sampler, a core storage chamber, an odor chamber, a behavior detection unit, and an observation device. Prior to the bioassays, the main behavioral detection unit was cleaned with ethanol and water, and the atmospheric sampler was operated for 15 min to remove any residual odors. Subsequently, 3-day-old *L. sticticalis* adults were acclimated in the testing room for 15 min, while 200 mg of freshly prepared FF, from which the solvent had evaporated, were placed in the odor chamber as the odor source. Another chamber containing FF without attractant served as the control. The behavior of the insects was observed by recording the number of insects found in the odor and control chambers.

The effect of FF with different release times on insect attraction was periodically tested under a fume hood. Each experiment included three replicates, with each replicate consisting of 30 male or female *L. sticticalis* adults. The insect behavior selection rate was calculated using Formula (2):

$$\begin{aligned}&\text{selection}\,rate\,(\%)\\&=\frac{Number\,of\,insects\,choosing\,the\,odor\,chamber}{Number\,of\,insects\,choosing\,the\,odor\,chamber\\+Number\,of\,insects\,choosing\,the\,control\,chamber}\end{aligned}\quad(2)$$

Trapping performance

During the *L. sticticalis* infestation period, field trapping experiments using FF loaded with food attractants were conducted in a *Pisum sativum* field located in Kangbao County, Zhangjiakou City, Hebei Province, China (41°52'3.77"N, 114°36'16.28"E). In this experiment, the attractant loading in the FF was 1 mg, and RS loaded with the same amount of attractant was used as the control group, with empty traps serving as the blank control (CK). Each sample was tested with six replicates. Freshly prepared FF were cut into strips and wrapped around both sides of the trap slots, while the commercial carriers were installed in the ring slots of the traps. The distance between traps was approximately 20 m. The positions of the traps were changed regularly to eliminate the interference of location factors on trapping. Trapping data were collected regularly, and pests were removed from the traps. Neither the attractants nor the traps were replaced during the entire experimental period.

Statistical analysis

OriginLab software was used to process data and curve fitting. For comparisons across multiple groups, one-way analysis of variance (ANOVA) was followed by Duncan's multiple range test. Different lowercase letters indicate significant differences between datasets, while $^{*}P<0.05$ denotes levels of statistical significance. ns indicates no significant difference. Each dataset is based on at least three independent experiments.

Results and discussions

Characterization of food attractant-loaded core-shell fibers

Core-shell structured fibers prepared via coaxial electrospinning are known for their excellent encapsulation of active ingredients [40], making them highly suitable for loading and releasing food attractants. In this study,

TEM images (Fig. 1A) of FF confirmed the successful formation of the core-shell structure, consistent with previous studies [41, 42]. Under LSM, the core and shell layers were loaded with different fluorescent dyes, which showed different fluorescence distribution (Figure S2), which further supported the emergence of core-shell structure. However, due to the limited difference in viscosity and surface tension between the core and shell spinning solutions, some variations in the core-shell structure occurred during the spinning process. Furthermore, this may also be attributed to changes in the electrospinning environment, such as temperature and humidity, as well as unstable voltage [43]. Overall, the diameter of FF was uniform and there was no obvious defective structure (Fig. 1B), which indicated that the Taylor cone had good stability during the spinning process. Statistics indicated that the average fiber diameter of FF was 1.39 ± 0.0456 μm, encompassing both nano- and micro-sized fibers (Fig. 1C). The uniformly arranged fiber structure of FF was also visible under an optical microscope (Fig. 1D). Therefore, it can be considered that the prepared core-shell spinning solution had good spinnability.

In the FTIR spectrum (Fig. 1E and Figure S3A), the peaks observed at 2882 cm^{-1} for PEO, 2941 cm^{-1} for PCL, and 2980 cm^{-1} for PHB correspond to C-H stretching vibrations. This was because these polymers had many -CH_2- groups and the related peaks also existed in FF. The peak at 1720 cm^{-1} was primarily attributed to C = O carbonyl stretching, and its presence in the FF spectrum was mainly due to the chemical structure of PCL and PHB [44]. The peak at 514 cm^{-1} may be attributed to the bending vibration of C-O. In addition to the absence of the characteristic peak of PEO, the peak at 1247 cm^{-1} for PHB/PCL fibers disappeared compared with FF, which may be due to the overlapping interference of the vibration modes of PEO with PHB/PCL. Notably, upon zooming in on the spectrum, an obvious peak at 1686 cm^{-1} was observed of the attractants, and this peak also appeared only in the FF (Figure S3B). This may be caused by the conjugation of C = C with C = O of unsaturated aldehydes or ketones [45], and the conjugation of aromatic rings with C = O of aromatic compounds [46]. In the UV spectrum (Fig. 1F), the peak at 230 nm of FF can be attributed to the presence of functional groups such as C = C, C = O, and benzene rings [47]. The absorption peak around 280 nm was primarily attributed to C = O functional groups. The π→π* transition absorption peak of unsaturated aldehydes and ketones may also be observed around 280 nm [48]. These results confirmed the successful loading of the food attractant onto the FF.

The XRD spectra indicated that PEO, PCL, and PHB each displayed crystallization peaks at the expected positions, and the overall crystallization intensity of FF significantly decreases after spinning (Fig. 1G). This occurred because the electrospinning process alters the polymer chain segment arrangement [49], causing the crystallization peaks of PCL and PEO, which were present in low content, to become less pronounced. XPS spectroscopy primarily examined surface chemical composition, and full spectrum analysis revealed that the surface of FF consists mainly of compounds containing carbon and oxygen (Figure S4). Deconvolution of high-resolution C1s and O1s spectra (Fig. 1H-M) revealed that the chemical bond compositions and contents related to carbon and oxygen on the FF surface closely matched those in PHB and PCL. Following electrospinning, the surface exposure of carbon and oxygen associated with C-O bonds in carboxyl groups on the fibers decreased, likely due to the orientation and rearrangement of polymer molecular chains [50]. No obvious chemical bonds associated with aldehydes, ketones, or aromatic rings were detected on the fiber surface, suggesting that food attractants were primarily loaded in the core layer of the micro-nano fibers. Consistent with previous research findings [37, 51], the TGA and DTG curves indicated that the weight loss of PHB began at 250 °C, that of PCL at 298 °C, and that of PEO at 351 °C (Figure S5). These thermogravimetric effects were also observed in FF, with the peak shifts compared to the pure materials attributed to the core-shell structure and the interactions between the components [52]. The thermal weight loss of the attractant began at 40 °C, with the peak decomposition rate occurring at 135 °C, which was not observed in FF loaded with attractant. This suggested that the encapsulation of FF enhanced the thermal stability of the original attractant.

Loading and release performance

In our strategy, the extracted food attractants are encapsulated within core-shell fibers made of multiple polymers to enhance the persistence of their efficacy in field applications (Fig. 2A). Prior to practical application, evaluating encapsulation/loading efficiency and analyzing release behavior are key steps. The encapsulation efficiencies of FF for 1-octen-3-ol, trans-2-hexenal, linalool, and anethole were 73.6%, 81.9%, 76.6%, and 82.0%, respectively (Fig. 2B), with an average encapsulation efficiency of 78.5%. The differences in encapsulation efficiency were related to the polarity of these compound molecules. The loading efficiencies of FF for 1-octen-3-ol, trans-2-hexenal, linalool, and anethole were 21.6%, 12.1%, 2.3%, and 2.4%, respectively, which were consistent with the initial ratio of food attractants. These results showed the outstanding encapsulation performance of the core-shell fibers, enabling different food attractants to work together to achieve a trapping effect in future applications. This also highlighted the chemical compatibility of

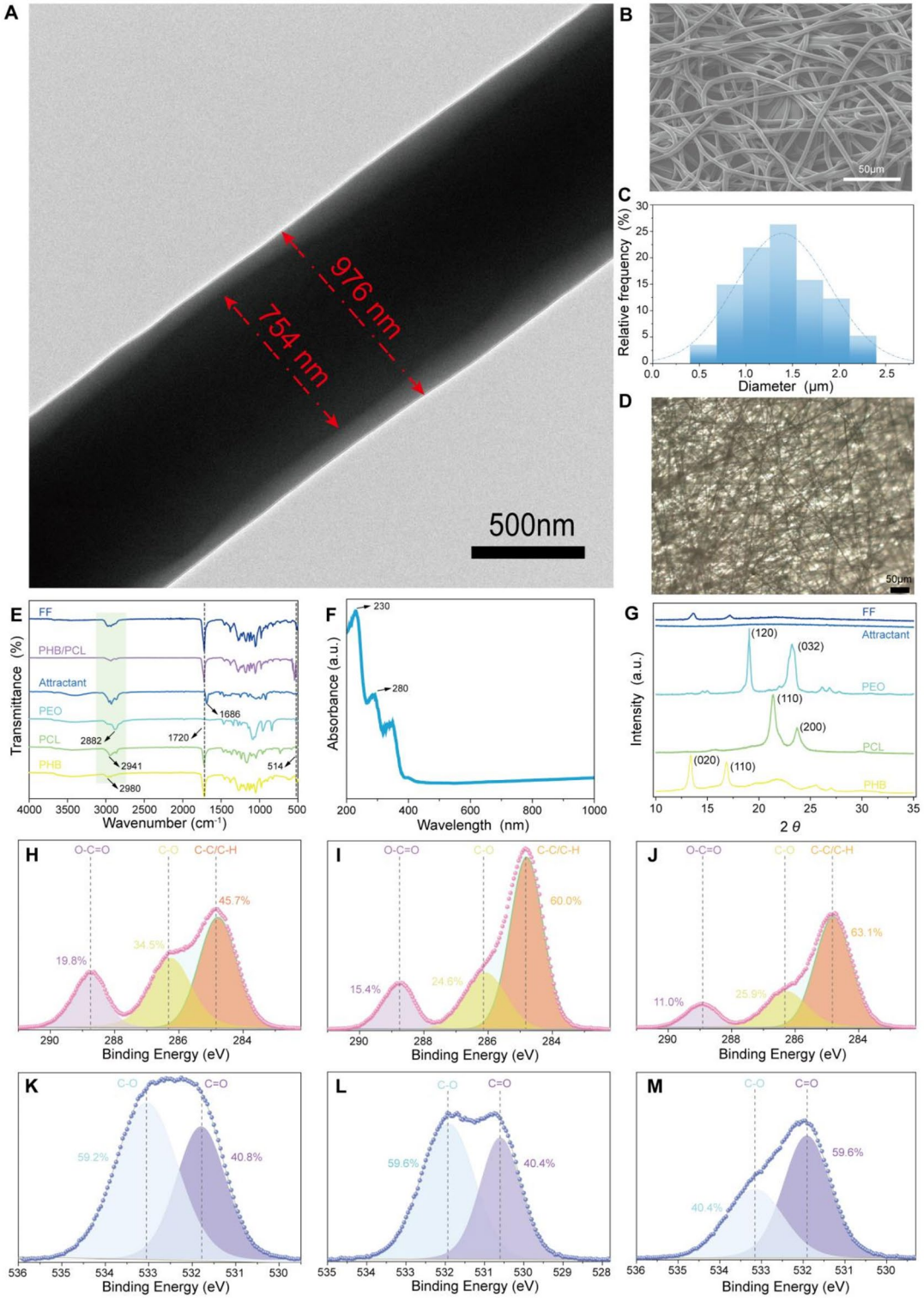

Fig. 1 FF characteristics. (**A**) TEM image. (**B**) SEM image. (**C**) Diameter statistical histogram. (**D**) Optical microscope image. (**E**) FTIR spectrum. (**F**) UV spectrum from 200 to 1000 nm. (**G**) XRD spectra. (**H-J**) XPS C1s spectra of PHB, PCL and FF. (**K-M**) XPS O1s spectra of PHB, PCL and FF

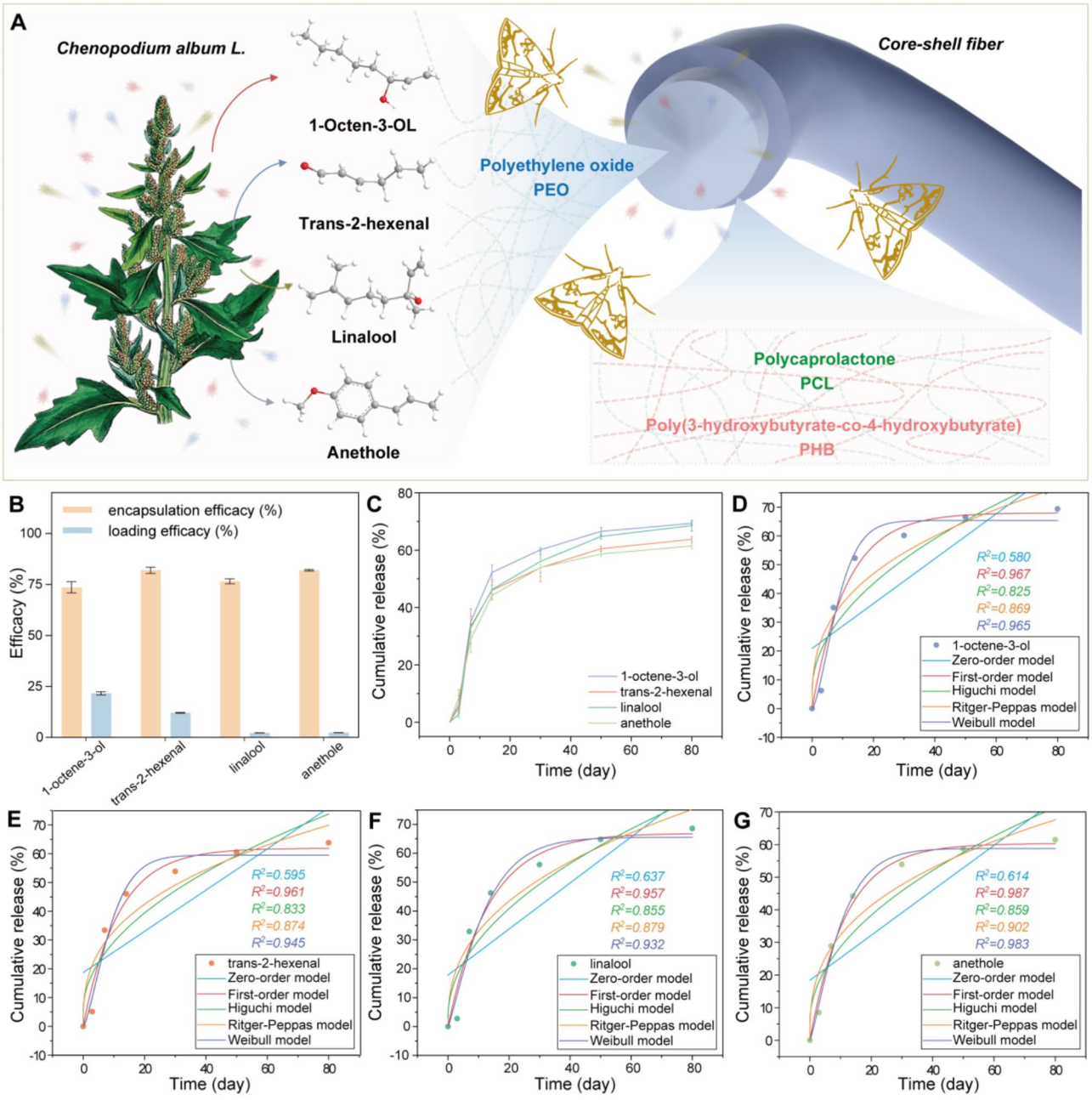

Fig. 2 Encapsulation and release behavior. (**A**) Schematic diagram of the use of core-shell fibers for loading food attractants and facilitating trapping. (**B**) Encapsulation and loading efficiency. (**C**) Release curves of the four compounds in FF. (**D**) Fitting results of the release curve of 1-octen-3-ol. (**E**) Fitting results of the release curve of trans-2-hexenal. (**F**) Fitting results of the release curve of linalool. (**G**) Fitting results of the release curve of anethole

PEO with food attractants, where van der Waals forces, electrostatic interactions, and hydrogen bonding, worked together to facilitate loading (Scheme 1). Indoor release curves indicated that the core-shell fiber only released just over 60% of all compounds within 80 days (Fig. 2C). The release time for this result was more than double that of our previous research [37], with the time to release 50% of the active ingredients also exceeding two weeks. Regarding this, alongside the performance advantage attributed to the core-shell structure, it is important to consider that the enhanced entanglement of molecular chains following the composite of PCL and PHB may hinder the diffusion of active molecules [53]. Furthermore, the retention of attractants in FF after 10 days of storage at different temperatures showed that higher temperatures significantly accelerated the release (Figure S6). More than 90% of the attractants were retained at 4 °C, indicating that FF was more suitable for storage

at low temperatures. Furthermore, the release rates of different compounds in FF increased with higher humidity, suggesting that a dry environment is beneficial for storage (Figure S7). Overall, the release performance of FF effectively mitigated the initial burst release of food attractants and significantly extended the sustained release duration.

The release curves of the four compounds were further fitted using five classical release models, with the first-order model demonstrating the highest degree of fit (Fig. 2D-G). The release of active ingredients from carriers, following a first-order release model, typically depended on time and initial concentration, with the release rate generally decreasing over time [54]. In practical applications, controlling the compound ratio is essential to ensure effective attraction [55]. All four compounds followed the first-order model, indicating similar release behaviors, which helped maintain a stable compound ratio throughout the release process. A detailed examination of the fitted release parameters for the four compounds revealed some differences among them (Table S2). The primary reasons for these differences included variations in molecular topological structure parameters, such as van der Waals volume, radius of gyration, and molecular weight [56]. Additionally, the positional distribution of molecules within the loaded micro-nano fibers should also be taken into account.

Stress resistance of FF

As previously mentioned, environmental factors in the field are the influencing factors of the effective duration of attractants [29, 57]. Bratinčević et al. [58] systematically analyzed and confirmed that factors such as temperature, humidity, wind speed, precipitation, air pressure, and cloud cover all changed the release of volatiles from slow-release dispensers. Our observations in the experimental field revealed that dew was present even within the traps (Fig. 3A), and direct contact with these water molecules could influence the release behavior of active molecules. Therefore, we incorporated PCL, which is

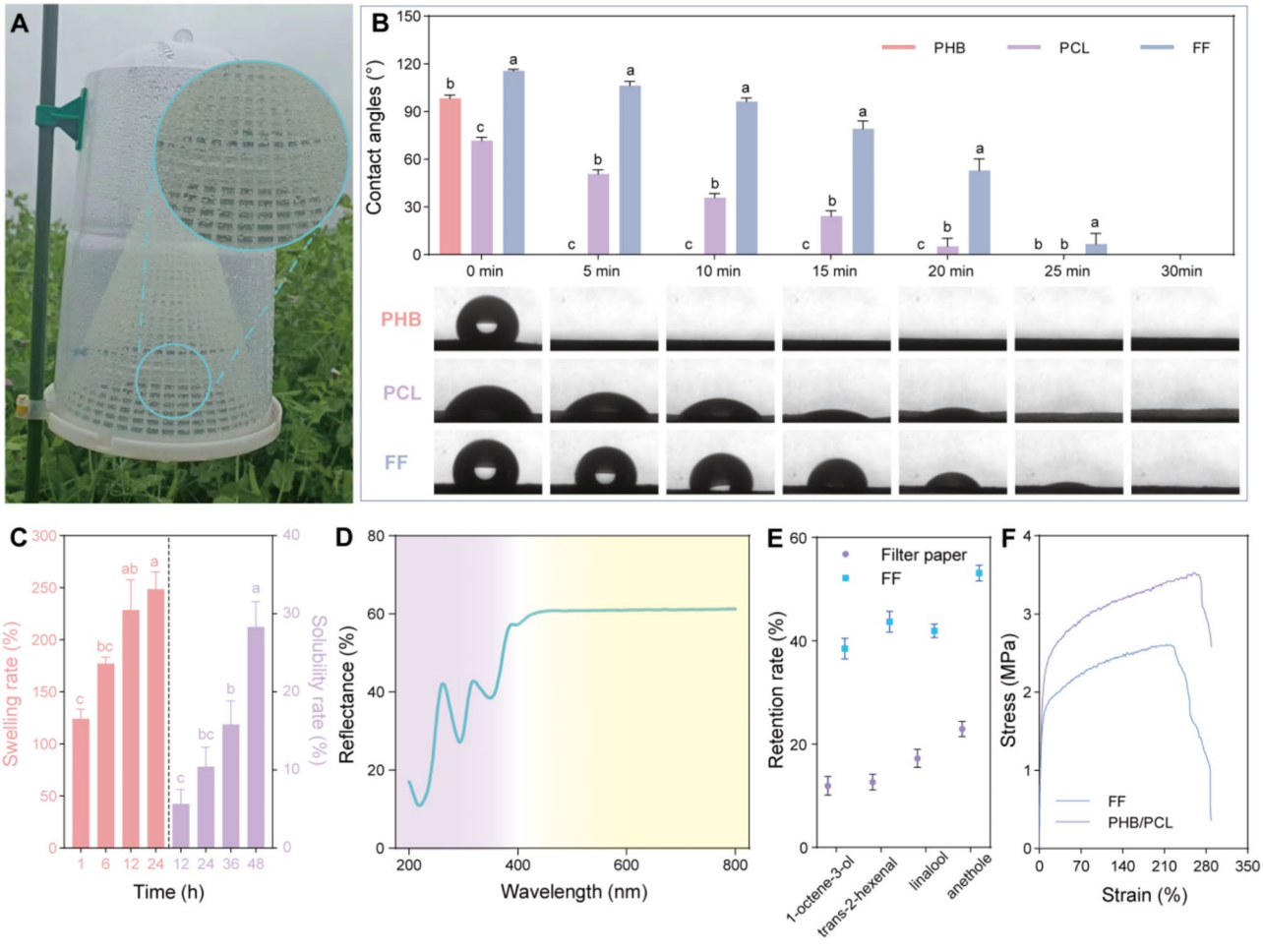

Fig. 3 Hydrophobicity, photostability and mechanical performance. (**A**) Photograph of the trap covered with dew during field use. (**B**) WCA of different mats and their changes over a 30-minute period. (**C**) Swelling and solubility rates of FF in water. (**D**) Reflection spectrum of FF. (**E**) Retention rate of attractant in FF after simulated UV aging. (**F**) Stress-strain curves of FF and PHB/PCL mats

more hydrophobic than PHB, to enhance the hydrophobicity of the core-shell fibers. The results indicated that the initial WCA of FF was approximately 116° (Fig. 3B), classifying it as a hydrophobic material. The WCA of 8% *w*/v PHB mats and 2% *w*/v PCL mats were 98.2° and 71.7°, respectively, indicating that the overall hydrophobicity of the PHB mat was enhanced upon compounding with PCL. In the WCA test lasting up to 30 min, FF exhibited water wetting behavior similar to PCL mat, with its WCA remaining above 90° during the first ten minutes. Good water resistance help protect the release of active molecules from FF. Considering the impact of environmental factors, we simulated the extreme scenario of FF being fully immersed in water to investigate its swelling and solubility behavior (Fig. 3C). Significant swelling of FF was observed within the first 6 h, while the rate of increase in swelling rate gradually leveled off after 12 h, which was related to the hydrophilicity of PEO. The solubility rate of FF within 24 h under vigorous stirring was about 10%, indicating that the FF structure had a certain water-resistance stability. However, the solubility increased significantly with longer immersion time, suggesting that the fiber structure of FF might be compromised.

UV reflectivity tests indicated that FF exhibited a reflectivity of 60% in the visible light range (400–700 nm), which can help mitigate direct sunlight exposure and subsequently reduce the temperature increase of the mat (Fig. 3D) [59]. This property contributes to mitigating the accelerated diffusion of active molecules induced by temperature. However, compared to the UV reflectivity of at least 70% achieved by fiber mats designed with specific molecular structures or composited with UV-resistant materials [60, 61], the reflectivity of FF in the UV range (200–400 nm) was relatively low. We further simulated the UV and condensation climate conditions in the field and tested the retention rate of attractants loaded on FF and common filter papers. The retention rates of various compounds in FF were approximately twice that in filter paper (Fig. 3E), which indicated that the core-shell fiber encapsulation structure of FF improved the UV resistance and weather resistance. However, compared to the normal release rate in Fig. 2C, UV exposure caused significant damage to the active molecules. Therefore, enhancing the UV reflectivity of the carrier is crucial to minimizing the risk of UV-induced oxidation of the active compounds.

Carrier materials with good mechanical properties can minimize unnecessary damage during application and transportation, thereby protecting the active ingredients contained within. As shown in the stress-strain curve in Fig. 3F, the elongation at break of FF was 289.34%, indicating that the material exhibited good toughness [62]. The tensile strength of FF was 2.6 MPa, which was higher than that of PVA-PEG [63], PCL-PEG [64], and PCL-chitosan [65] with the core-shell structure reported in pervious literature. Compared with PHB/PCL mats, the mechanical properties of FF were weakened, likely due to the introduction of the PEO material. Nevertheless, FF demonstrated a strong ability to resist external damage, enhancing its potential for application.

Degradability of FF

Currently, microplastic pollution in agricultural land is a growing concern, and efforts worldwide are underway to promote the adoption and enforcement of anti-plastic policies [66]. This suggested that difficult-to-degrade sustained-release carriers, such as polyethylene and polyvinyl chloride plastics, may face strict restrictions in this application field. Therefore, we selected widely studied degradable polymers as carrier materials in this study to align with goals for sustainable agricultural development. As shown in Fig. 4A, the degradation of FF and RS was evaluated through composting experiments. In contrast, FF was degraded by more than 3% within a week, while RS showed minimal change, with significant differences in their degradation rate (Fig. 4B). The FTIR spectrum of FF showed that, with increasing degradation time, the peak at 1720 cm^{-1}, representing the C = O group, shifted and weakened, while the breakdown of original chemical bonds resulted in the emergence of additional small absorption peaks (Fig. 4C). These phenomena were consistent with the biodegradation results of similar materials reported previously [67, 68]. Figure 4D showed that, under the influence of microorganisms, the fiber surface was gradually eroded, and its overall roughness increased. These results indicated that FF exhibited good biodegradability in soil and could serve as a greener agricultural input compared to petroleum-based plastics.

In a realistic scenario simulating continuous field application, we examined the natural degradation of FF in air by SEM. By the 30th day of field application, noticeable areas of diameter reduction were observed in the fibers of FF, with the number of these areas increasing over time (Fig. 4E). Statistical analysis of fiber diameters indicated that the average fiber diameter of FF gradually decreased from approximately 1.2 μm on 30th day to about 900 nm by 120th. This suggested that the fibers degraded gradually, with their diameter reducing over time during use. In terms of release, the morphology and structure of FF remained relatively unchanged in the initial stage (before 30 days), with PHB/PCL serving as a protective barrier to prevent the early burst release of active molecules. In the later stage, the ongoing degradation of FF prevented the issue of tailing release of active molecules, ensuring complete release.

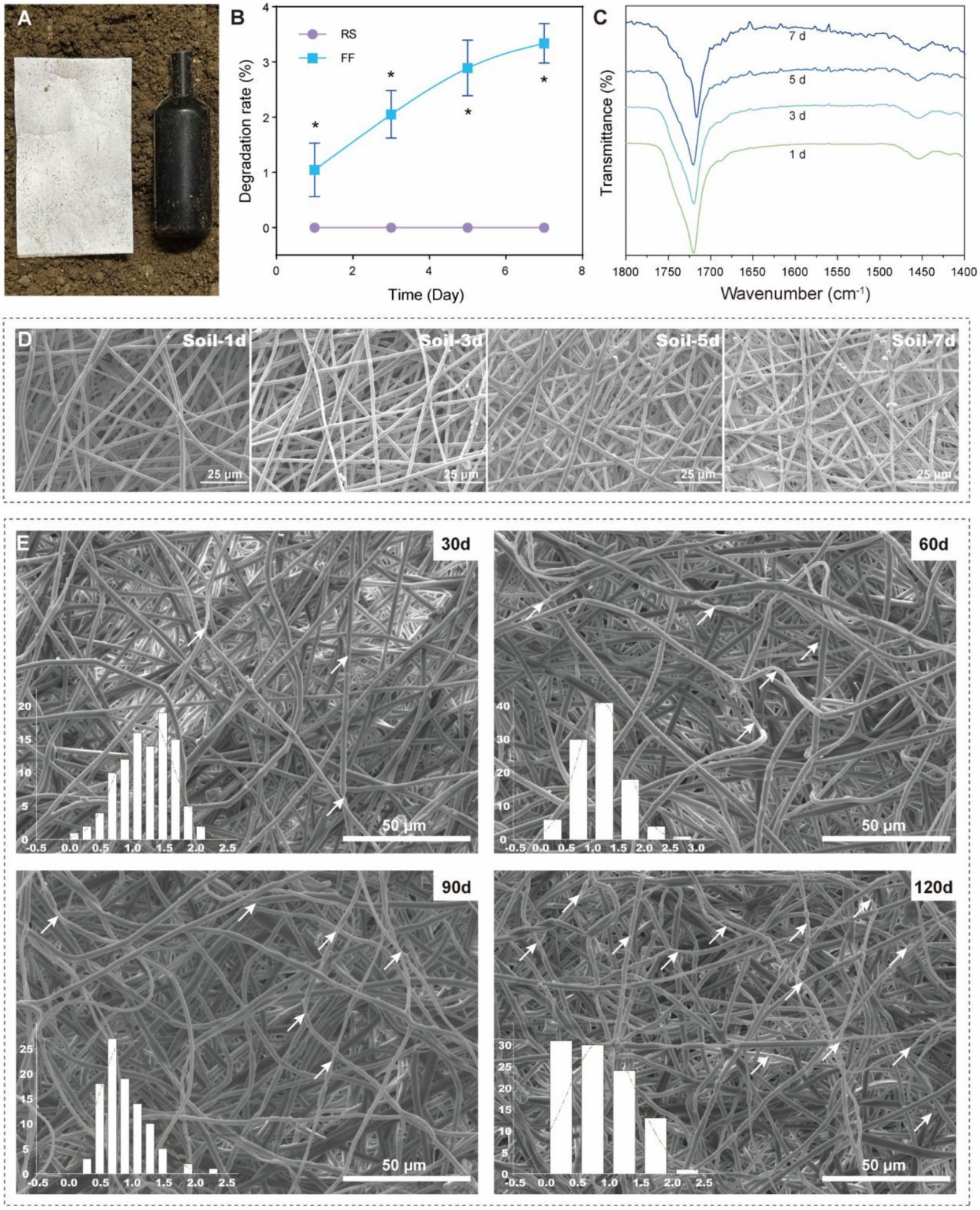

Fig. 4 Degradation performance. (**A**) Schematic diagram of the composting experiment, with FF on the left and RS on the right. (**B**) Degradation rate curve. (**C**) FTIR spectrum of FF with different degradation days. (**D**) SEM images of FF with different degradation days. (**E**) The degradation effect during actual use is shown by SEM (the white arrow indicates the area with shortened diameter)

Research on EAG and insect behavior

Long-term research indicates that a release system designed for sustained attraction to insects must not only account for the duration of release but also consider the relationship between release concentration, ratio, and the insect response threshold [36, 55, 69]. To evaluate the effectiveness of the food attractant released by the slow-release FF against the *L. sticticalis*, we assessed the electrophysiological (Fig. 5A) of the *L. sticticalis* every 15 days over a 90-day period. The EAG results (Fig. 5B) indicated that the freshly prepared FF elicited the strongest stimulation in both male and female adults, and subsequently decreased over time. The response intensity for male adults was 2.87 mV, surpassing that of female adults, which was 2.38 mV. However, the EAG response intensity showed no significant difference between males and females, confirming the long-term stable bisexual attraction ability of FF. Notably, 90 days post-release, the EAG responses of both male and female adults to FF persisted, decreasing to 1.38 mV and 1.35 mV, respectively.

Assessing insect behavioral responses is essential for evaluating attractant effectiveness. Herein, we used an insect olfactory behavior selection apparatus (Fig. 5C) to test FF. The results showed that FF significantly induced behavioral responses in both male and female *L. sticticalis*. Compared to the fiber mat without food attractants, FF maintains its attractive effect on both male and female adults of *L. sticticalis* for at least 75 days. The behavioral responses observed on the 90th day suggested that the release concentration of the FF attractant was insufficient to attract insects (Fig. 5D-E). The duration of action observed in the biological activity and insect behavior studies aligned closely with the results from the indoor release test, confirming that FF can achieve sustained and effective release. These results also supported the further research of FF for field applications.

Trapping performance at field

The four food attractant compounds selected in this study were derived from host plants of *L. sticticalis* and have shown high attractiveness to *L. sticticalis* in field settings. Therefore, a key step in verifying the effectiveness of the "attractive substitution strategy" is to conduct real field experiments. To further assess the field trapping efficacy of FF against *L. sticticalis*, a trapping test was conducted using a commercially available conventional trap fitted with the FF (Fig. 6A). The FF used in the field exhibited a trapping trend similar to that of the commercially available RS (Fig. 6B). However, the daily number of FF traps was higher than that of CK and RS for most of the time, with a significant difference observed on the 13th day. Previous research and investigation results suggested that the enhanced trapping efficacy of fiber carriers may be attributed to the uniform distribution of active molecules facilitated by the micro-nano structure [29, 33]. FF reached its trapping peak on the 8th day and subsequently declined, which may be attributed to the migratory habits of *L. sticticalis* [70], resulting in an overall reduction of the insect population in the surveyed fields. During the entire trapping period, each trap equipped with FF captured 22 males and 25 females, both of which were higher than the numbers captured by RS (Fig. 6C). The absence of significant differences in the number of male and female adults captured by FF indicated that FF effectively achieved strong bisexual attraction in the field. In short, the micro-nano fiber carrier with a core-shell structure exhibited superior trapping efficacy and field adaptability compared to the RS.

Conclusions

In this study, coaxial electrospinning technology was successfully used to construct a micro-nano fiber mat loaded with food attractants, including 1-octen-3-ol, trans-2-hexenal, linalool, and anethole, designed for the bisexual attraction of *L. sticticalis*. Analysis of the physical and chemical properties indicated that the multiple polymers exhibited good chemical compatibility, successfully formed a bead-free mat with core-shell structure, and effectively encapsulated the active molecules of the food attractant within the fiber core. The key advantage of this micro-nano structure is its ability to efficiently encapsulate multiple active molecules simultaneously, mitigate burst release, and achieve sustained release. The long-term efficacy of food attractants released by FF was thoroughly validated through biological activity and insect behavior experiments. Moreover, the prepared FF exhibited hydrophobicity, photostability, mechanical strength, and degradability, effectively protecting active molecules and aligning with the goals of sustainable agricultural development. Importantly, FF was successfully applied in the field to trap *L. sticticalis*, demonstrating a significantly better bisexual trapping effect than the RS. However, due to the insect migration, this study was unable to conduct long-term trapping monitoring. Future proof-of-concept studies should be conducted over a longer time scale. In addition, given the complexity of the field environment, factors such as rainfall, ultraviolet radiation, high temperatures, ozone levels, and wind speed should all be evaluated more comprehensively. In conclusion, core-shell micro-nano fiber mats constructed from environmentally polymers enable effective encapsulation, sustained release, and practical field application of food attractants. This research offers an innovative strategy for the efficient and precise application of green alternatives to traditional pesticides.

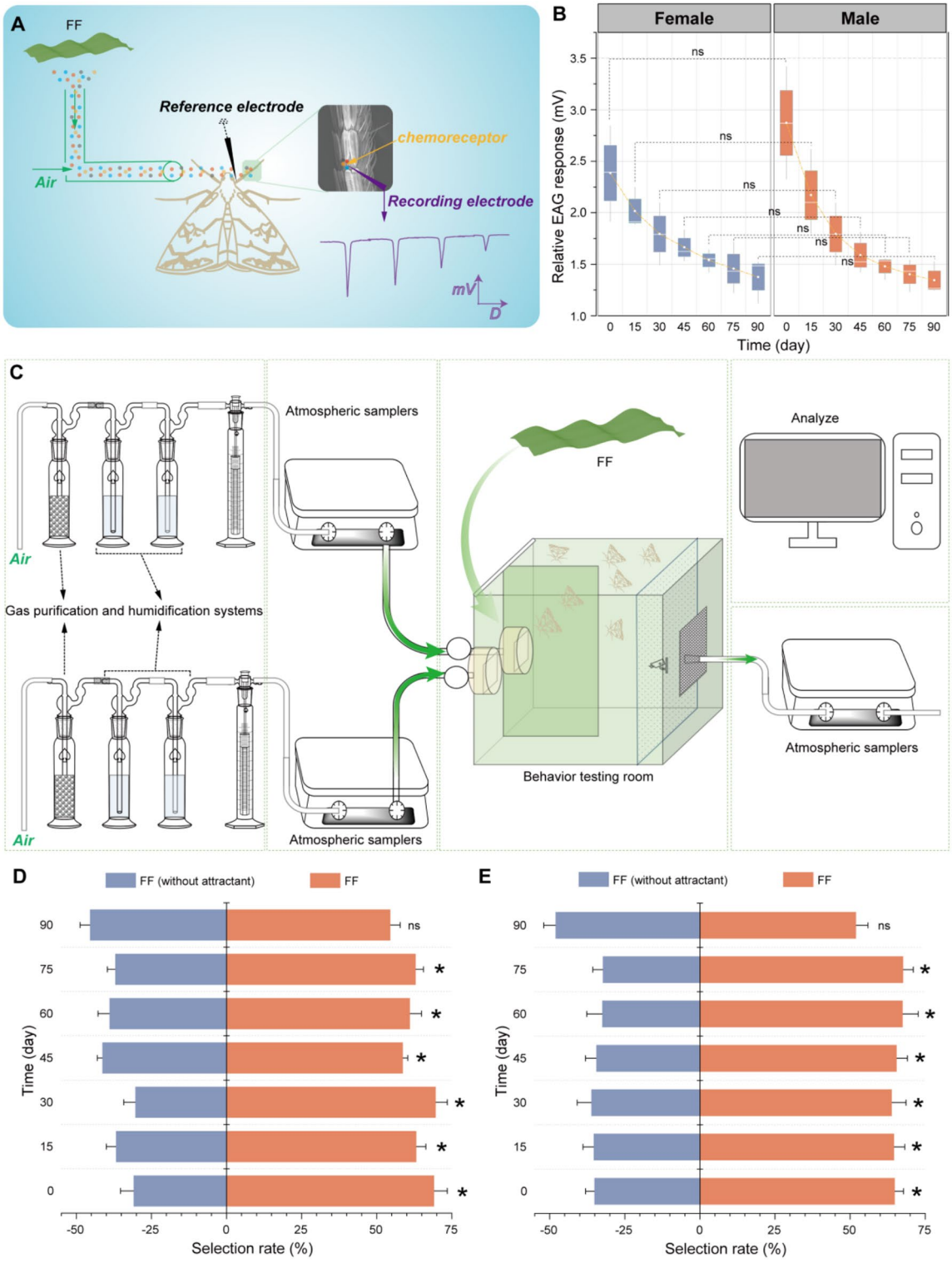

Fig. 5 Biological activity of FF. (**A**) Schematic diagram of the electrophysiological responses of *L. sticticalis* as recorded by the EAG device. **(B**) The variation in the intensity of EAG responses of adult *L. sticticalis* to food attractants released by FF at different time points. (**C**) Insect olfactory behavior selection apparatus. The attractant effect of FF on female (**D**) and male (**E**) adults at different time points of food attractant release

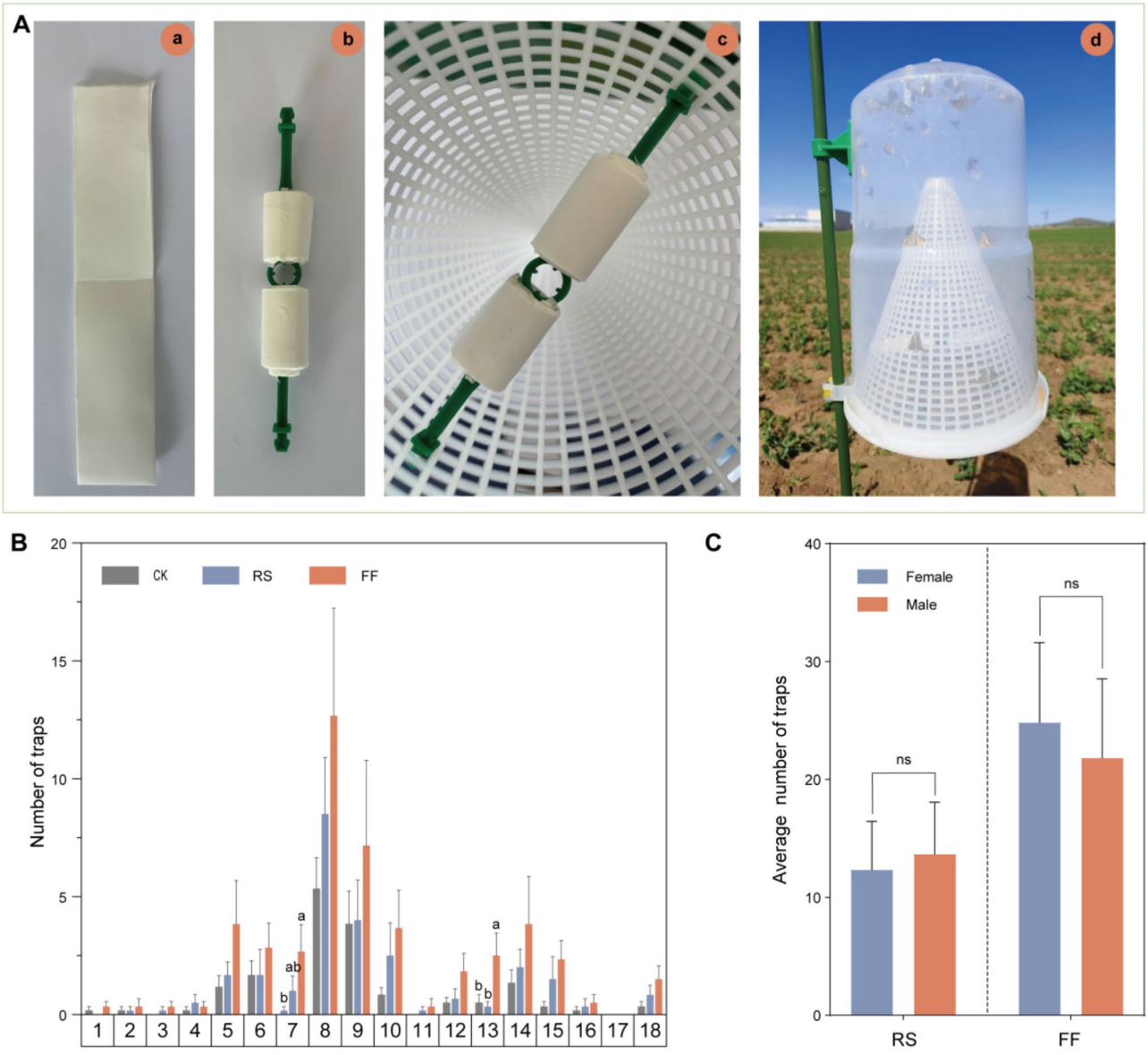

Fig. 6 Field application and trapping effect of FF. (**A**) Procedure for traps equipped with FF. (a) Cut FF into strips. (b) Wrapped around both sides of the trap slot. (c) Installed in the trap. (d) Used in the field. (**B**) The number of traps for CK, RS, and FF at different time points. (**C**) The total number of male and female adults trapped by RS and FF

Supplementary Information

The online version contains supplementary material available at https://doi.org/10.1186/s12951-025-03269-2.

Supplementary Material 1

Acknowledgements
The authors gratefully acknowledge Mingqing Wang for providing adult *L. sticticalis* used in this study. Special thanks are extended to Aiguo Kang for his invaluable guidance on the field trapping experiments with fiber films. Their contributions were instrumental to the success of this research.

Author contributions
Chenglong Cui and Wenjie Shangguan made equal contributions to this work. Chenglong Cui took charge of methodology, software, and data analysis. Wenjie Shangguan focused on writing the original draft, investigation, and formal analysis. Kebin Li, Xingfu Jiang and Zhimin Wang contributed to the validation and review of the manuscript. Jiao Yin and Lidong Cao played major roles in project administration, supervision, validation, resources, as well as writing, reviewing, and editing the manuscript. All authors have read and approved the final manuscript.

Funding
This work was financially supported by the National Key Research Development Program of China (2022YFD1400600) and the National Natural Science Foundation of China (32472618).

Data availability
No datasets were generated or analysed during the current study.

Declarations

Ethics approval and consent to participate
Not applicable.

Consent for publication
All authors are agreed to publish this paper.

Competing interests
The authors declare no competing interests.

Author details
[1]State Key Laboratory for Biology of Plant Diseases and Insect Pests, Institute of Plant Protection of Chinese Academy of Agricultural Sciences, No. 2 Yuanmingyuan West Road, Haidian District, Beijing 100193, PR China

Received: 2 January 2025 / Accepted: 24 February 2025
Published online: 01 April 2025

References

1. Tang FHM, Lenzen M, McBratney A, Maggi F. Risk of pesticide pollution at the global scale. Nat Geosci. 2021;14(4):206–10.
2. Gould F, Brown ZS, Kuzma J. Wicked evolution: can we address the Sociobiological dilemma of pesticide resistance? Science. 2018;360(6390):728–32.
3. Yang Y, Tilman D, Jin Z, Smith P, Barrett CB, Zhu YG, Burney J, D'Odorico P, Fantke P, Fargione J, et al. Climate change exacerbates the environmental impacts of agriculture. Science. 2024;385(6713):eadn3747.
4. Schulz R, Bub S, Petschick LL, Stehle S, Wolfram J. Applied pesticide toxicity shifts toward plants and invertebrates even in GM crops. Science. 2021;372(6537):81–4.
5. Nicholson CC, Knapp J, Kiljanek T, Albrecht M, Chauzat MP, Costa C, De la Rua P, Klein AM, Mand M, Potts SG, et al. Pesticide use negatively affects bumble bees across European landscapes. Nature. 2024;628(8007):355–8.
6. Gandara L, Jacoby R, Laurent F, Spatuzzi M, Vlachopoulos N, Borst NO, Ekmen G, Potel CM, Garrido-Rodriguez M, Böhmert AL, et al. Pervasive sublethal effects of agrochemicals on insects at environmentally relevant concentrations. Science. 2024;386(6720):446–53.
7. Hough RL. A world view of pesticides. Nat Geosci. 2021;14(4):183–84.
8. Huang SZ, Zhang L, Xie DJ, Tang JH, Jiang YY, Mijidsuren B, Baasan M, Luo LZ, Jiang XF. Transboundary migration of Loxostege sticticalis (Lepidoptera: Crambidae) among China Russia and Mongolia. Pest Manage Sci. 2024;80(9):4650–64.
9. Pinniger DB. Food-Baited traps; past present and future. J Kans Entomol Soc. 1990;63(4):533–8.
10. Epsky ND, Kendra PE, Schnell EQ. History and Development of Food-Based Attractants. In Trapping and the Detection Control and Regulation of Tephritid Fruit Flies: Lures Area-Wide Programs and Trade Implications. Shelly T, Epsky N, Jang E B, Reyes-Flores J, Vargas R. EdsSpringer Netherlands. 2014; pp 75–118.
11. Wang L, He L, Wang T, Xiao T, Zou Z, Wang M, Cai X, Yao B, Yang Y, Wu K. The effectiveness of mixed food attractant for managing Helicoverpa armigera (Hübner) and Agrotis ipsilon (Hufnagel) in peanut fields. Agronomy. 2024;14(5):986.
12. Epsky ND, Heath RR, Guzman A, Meyer WL. Visual cue and chemical cue interactions in a dry trap with Food–Based synthetic attractant for Ceratitis capitata and Anastrepha ludens (Diptera: Tephritidae). Environ Entomol. 1995;24(6):1387–95.
13. Candia IF, Bautista V, Larsson Herrera S, Walter A, Ortuno Castro N, Tasin M, Dekker T. Potential of locally sustainable food baits and traps against the mediterranean fruit fly Ceratitis capitata in Bolivia. Pest Manage Sci. 2019;75(6):1671–80.
14. Garcia-Martinez MA, Presa-Parra E, Valenzuela-Gonzalez JE, Lasa R. The fruit fly lure ceratrap: an effective tool for the study of the arboreal ant fauna (Hymenoptera: Formicidae). J Insect Sci. 2018;18(4):16.
15. Sabier M, Wang J, Zhang T, Jin J, Wang Z, Shen B, Deng J, Liu X, Zhou G. The attractiveness of a food based lure and its component volatiles to the stored-grain pest Oryzaephilus surinamensis (L). J Stored Prod Res. 2022;98:102000.
16. Álvarez G, Gallego D, Hall DR, Jactel H, Pajares JA. Combining pheromone and Kairomones for effective trapping of the pine Sawyer beetle Monochamus galloprovincialis. J Appl Entomol. 2016;140(1–2):58–71.
17. Meiners T. Chemical ecology and evolution of plant-insect interactions: a multitrophic perspective. Curr Opin Insect Sci. 2015;8:22–8.
18. Loreto F, D'Auria S. How do plants sense volatiles sent by other plants? Trends Plant Sci. 2022;27(1):29–38.
19. Deng JY, Wei HY, Huang YP, Du JW. Enhancement of attraction to sex pheromones of Spodoptera exigua by volatile compounds produced by host plants. J Chem Ecol. 2004;30(10):2037–45.
20. Chi DT, Thi HL, Vang LV, Thy TT, Yamamoto M, Ando T. Mass trapping of the Diamondback moth (Plutella Xylostella L.) by a combination of its sex pheromone and allyl isothiocyanate in cabbage fields in Southern Vietnam. J Pestic Sci. 2024;49(1):15–21.
21. Nielsen M-C, Sansom CE, Larsen L, Worner SP, Rostás M, Chapman RB, Butler RC, de Kogel WJ, Davidson MM, Perry NB, et al. Volatile compounds as insect lures: factors affecting release from passive dispenser systems. N Z J Crop Hortic Sci. 2019;47(3):208–23.
22. Sun C, Wang A, Shen Y, Li X, Zhan S, Wang C, Verheggen F, Wang Y. Innovative matrices to release pheromones for integrated pest management. Entomol Gen. 2024;44(5):113544.
23. Pavela R, Benelli G. Essential oils as ecofriendly biopesticides?? Challenges and constraints. Trends Plant Sci. 2016;21(12):1000–7.
24. Sharifi R, Ryu C-M. Formulation and agricultural application of bacterial volatile compounds. in bacterial volatile compounds as mediators of airborne interactions Ryu C-M. Weisskopf L. Piechulla B Eds., Springer Singapore. 2020; pp 317–336.
25. Gregg PC, Del Socorro AP, Hawes AJ, Binns MR. Developing bisexual Attract-and-Kill for polyphagous insects: ecological rationale versus pragmatics. J Chem Ecol. 2016;42(7):666–75.
26. Light DM, Beck JJ. Characterization of microencapsulated Pear ester (2E,4Z)-ethyl-2,4-decadienoate, a kairomonal spray adjuvant against neonate codling moth larvae. J Agric Food Chem. 2010;58(13):7838–45.
27. Bian L, Sun XL, Cai XM, Chen ZM. Slow release of plant volatiles using Sol-Gel dispensers. J Econ Entomol. 2014;107(6):2023–9.
28. Mun H, Townley HE. Nanoencapsulation of plant volatile organic compounds to improve their biological activities. Planta Med. 2021;87(3):236–51.
29. Hellmann C, Greiner A, Vilcinskas A. Design of polymer carriers for optimized pheromone release in sustainable insect control strategies. Adv Sci. 2023;11(9):e2304098.
30. Ji D, Lin Y, Guo X, Ramasubramanian B, Wang R, Radacsi N, Jose R, Qin X, Ramakrishna S. Electrospinning of nanofibres. Nat Rev Methods Primers. 2024;4:1.
31. Greiner A, Wendorff JH. Electrospinning: a fascinating method for the Preparation of ultrathin fibers. Angew Chem Int Ed Engl. 2007;46(30):5670–703.
32. Kong B, Liu R, Guo J, Lu L, Zhou Q, Zhao Y. Tailoring micro/nano-fibers for biomedical applications. Bioact Mater. 2023;19:328–47.
33. Shangguan WJ, Mei XD, Chen HP, Shuai H, Xu CL, Wang L, Lv KF, Huang QL, Xu HL, Cao LD. Biodegradable electrospun fibers as Sustained-Release carriers of insect pheromones for field trapping of Spodoptera litura (Lepidoptera: Noctuidae). Pest Manage Sci. 2023;79:4774–83.
34. Kikionis S, Ioannou E, Konstantopoulou M, Roussis V. Electrospun micro/nanofibers as controlled release systems for pheromones of Bactrocera oleae and prays oleae. J Chem Ecol. 2017;43(3):254–62.
35. Qian Y, Zhang J, Yu Y, Jiang Q, Yan B, Song X, Yu X, Cheng Z. Preparation of long-lasting releasing Methyl Eugenol fiber membrane and its trapping analysis on Bactrocera dorsalis. Polymer. 2023;285(20):126349.
36. De Czarnobai B, Bisotto-de-Oliveira R, Pereira CN, Sant'Ana J. Novel nanoscale pheromone dispenser for more accurate evaluation of grapholita molesta (Lepidoptera: Tortricidae) attract-and-kill strategies in the laboratory. Pest Manage Sci. 2017;73(9):1921–6.
37. Shangguan W, Xu H, Ding W, Chen H, Mei X, Zhao P, Cao C, Huang Q, Cao L. Nano-Micro Core–Shell fibers for efficient pest trapping. Nano Lett. 2023;23(24):11809–17.
38. Xue J, Wu T, Dai Y, Xia Y. Electrospinning and electrospun nanofibers: methods materials and applications. Chem Rev. 2019;119(8):5298–415.
39. Ullah A, Sun L, Wang F-f, Nawaz H, Yamashita K, Cai Y, Anwar F, Khan MQ, Mayakrishnan G, Kim IS. Eco-friendly bioactive β-caryophyllene/halloysite nanotubes loaded nanofibrous sheets for active food packaging. Food Packag Shelf Life. 2023;35:101028.
40. Loscertales IG, Barrero A, Guerrero I, Cortijo R, Marquez M, Ganan-Calvo AM. Micro/nano encapsulation via electrified coaxial liquid jets. Science. 2002;295(5560):1695–8.
41. Li H, Wong SY, Zhang Y, Sim JY, Lu Y, Yu Y, Li D, Li X. Humidity-responsive antimicrobial properties of EVOH nanofibers loaded with cuminaldehyde/

HβCD inclusion complexes and its application in chicken preservation. Food Hydrocoll. 2024;150:109749.
42. Tan R, Zhang K, Si Y, Zhang S, Yang J, Hu J. Implantable Epigallocatechin gallate Sustained-Release nanofibers for the prevention of Immobilization-Induced muscle atrophy. ACS Nano. 2023;18(1):919–30.
43. Sun Z, Zussman E, Yarin AL, Wendorff JH, Greiner A. Compound Core–Shell polymer nanofibers by Co-Electrospinning. Adv Mater. 2003;15(22):1929–32.
44. Eskitoros-Togay ŞM, Bulbul YE, Dilsiz N. Quercetin-loaded and unloaded electrospun membranes: synthesis characterization and in vitro release study. J Drug Deliv Sci Technol. 2018;47:22–30.
45. Lindenmaier R, Williams SD, Sams RL, Johnson TJ. Quantitative infrared Absorption spectra and vibrational assignments of Crotonaldehyde and Methyl vinyl ketone using Gas-Phase Mid-Infrared Far-Infrared and liquid Raman spectra: s-cis vs s-trans composition confirmed via temperature studies and Ab initio methods. J Phys Chem A. 2017;121(6):1195–212.
46. Wang Q, Ye J-b, Yang H-y, Liu Q. Chemical composition and structural characteristics of oil shales and their kerogens using fourier transform infrared (FTIR) spectroscopy and Solid-State 13 C nuclear magnetic resonance (NMR). Energy Fuel. 2016;30(8):6271–80.
47. Fleming I, Williams D. Ultraviolet and visible spectra. In: Williams D, editor. Spectroscopic methods in organic chemistry Fleming I. Springer International Publishing; 2019. pp. 55–83.
48. Kalsi P. Spectroscopy of organic compounds. New age international. 2007.
49. Izumikawa S, Yoshioka S, Aso Y, Takeda Y. Preparation of poly(l-lactide) microspheres of different crystalline morphology and effect of crystalline morphology on drug release rate. J Control Release. 1991;15(2):133–40.
50. Zander NE, Orlicki JA, Rawlett AM, Beebe TP Jr. Quantification of protein incorporated into electrospun Polycaprolactone tissue engineering scaffolds. ACS Appl Mater Interfaces. 2012;4(4):2074–81.
51. Negahdari N, Alizadeh S, Majidi J, Saeed M, Ghadimi T, Tahermanesh K, Arabsorkhi-Mishabi A, Pezeshki-Modaress M. Heat-treated alginate-polycaprolactone core-shell nanofibers by emulsion electrospinning process for biomedical applications. Int J Biol Macromol. 2024;275(Pt 2):133709.
52. Pakravan M, Heuzey MC, Ajji A. Core-shell structured PEO-chitosan nanofibers by coaxial electrospinning. Biomacromolecules. 2012;13(2):412–21.
53. Ding Y, Roether JA, Boccaccini AR, Schubert DW. Fabrication of electrospun Poly (3-hydroxybutyrate)/poly (ε-caprolactone)/silica hybrid fibermats with and without calcium addition. Eur Polym J. 2014;55:222–34.
54. Karimi Alavijeh R, Akhbari K, Biocompatible. MIL-101(Fe) as a smart carrier with high loading potential and sustained release of Curcumin. Inorg Chem. 2020;59(6):3570–78.
55. Kuzmich D, Kawagoe ZA, Walse SS. PVC formulation of Anastrepha suspensa pheromones suitable for field studies. Engineering. 2021;7(11):1646–50.
56. Zhang R, Wen LY, Wu WS, Yuan XZ, Zhang LJ. Quantitative Structure-Property relationship for pH-Triggered drug release performance of Acid-Responsive Four/Six-Arms star polymeric micelles. Pharm Res. 2018;36(1):20.
57. Jiang NJ, Dong X, Veit D, Hansson BS, Knaden M. Elevated Ozone disrupts mating boundaries in drosophilid flies. Nat Commun. 2024;15(1):2872.
58. Versic Bratincevic M, Bego A, Nizetic Kosovic I, Jukic Spika M, Burul F, Popovic M, Nincevic Runjic T, Vitanovic E. A lifetime of a Dispenser-Release rates of Olive fruit fly-Associated yeast volatile compounds and their influence on Olive fruit fly (Bactrocera Oleae Rossi) attraction. Molecules. 2023;28(6):2431.
59. Wu R, Sui C, Chen T-H, Zhou Z, Li Q, Yan G, Han Y, Liang J, Hung P-J, Luo E, et al. Spectrally engineered textile for radiative cooling against urban heat Islands. Science. 2024;384(6701):1203–12.
60. Li M, Yan Z, Fan D. Flexible radiative cooling textiles based on composite nanoporous fibers for personal thermal management. ACS Appl Mater Interfaces. 2023;15(14):17848–57.
61. Peng Y, Dong J, Long J, Zhang Y, Tang X, Lin X, Liu H, Liu T, Fan W, Liu T, et al. Thermally conductive and UV-EMI shielding electronic textiles for unrestricted and multifaceted health monitoring. Nanomicro Lett. 2024;16(1):199.
62. Yeo JCC, Muiruri JK, Tan BH, Thitsartarn W, Kong J, Zhang X, Li Z, He C. Biodegradable PHB-Rubber copolymer toughened PLA green composites with ultrahigh extensibility. ACS Sustain Chem Eng. 2018;6(11):15517–27.
63. Kan Y, Bondareva JV, Statnik ES, Cvjetinovic J, Lipovskikh S, Abdurashitov AS, Kirsanova MA, Sukhorukhov GB, Evlashin SA, Salimon AI, et al. Effect of graphene oxide and Nanosilica modifications on electrospun Core-Shell PVA-PEG-SiO(2)@PVA-GO Fiber Mats. Nanomaterials. 2022;12(6):998.
64. Mahdieh Z, Mitra S, Holian A. Core–Shell electrospun fibers with an improved open pore structure for Size-Controlled delivery of nanoparticles. ACS Appl Polym Mater. 2020;2(9):4004–15.
65. Surucu S, Turkoglu Sasmazel H. Development of core-shell coaxially electrospun composite PCL/chitosan scaffolds. Int J Biol Macromol. 2016;92:321–8.
66. He L, Li Z, Jia Q, Xu Z. Soil microplastics pollution in agriculture. Science. 2023;379(6632):547.
67. Mousavioun P, George GA, Doherty WOS. Environmental degradation of lignin/poly(hydroxybutyrate) blends. Polym Degrad Stab. 2012;97(7):1114–22.
68. Sun Y, Shaheen SM, Ali EF, Abdelrahman H, Sarkar B, Song H, Rinklebe J, Ren X, Zhang Z, Wang Q. Enhancing microplastics biodegradation during composting using livestock manure Biochar. Environ Pollut. 2022;306:119339.
69. Wang H-L, Ding B-J, Dai J-Q, Nazarenus TJ, Borges R, Mafra-Neto A, Cahoon EB, Hofvander P, Stymne S, Löfstedt C. Insect pest management with sex pheromone precursors from engineered oilseed plants. Nat Sustain. 2022;5(11):981–90.
70. Feng H, Wu K, Cheng D, Guo Y. Spring migration and summer dispersal OfLoxostege sticticalis(Lepidoptera: Pyralidae) and Other Insects Observed with Radar in Northern China. Environ Entomol. 2004;33(5):1253–65.

Publisher's note